PROCEEDINGS OF SCIENCE

# Exploring the Universe's Extreme Events: Galactic Transients at High and Very High Energies

**Daniela Hadasch**[a,*]

[a] *Institute for Cosmic Ray Research (ICRR), The University of Tokyo, 5-1-5 Kashiwanoha, Kashiwa, Chiba, 277-8582, Japan*

*E-mail:* hadasch@icrr.u-tokyo.ac.jp

Transient phenomena in the Milky Way emit radiation across the electromagnetic spectrum and are essential for understanding the extreme astrophysical processes that occur in our galaxy. At high and very high energies (HE and VHE), these events can provide valuable insights into the acceleration mechanisms of particles, the interstellar medium, and the astrophysical processes driving these phenomena.

Recent observations from $\gamma$-ray telescopes like *Fermi*-LAT, H.E.S.S., MAGIC, and VERITAS have led to the detection and characterization of various types of HE and VHE transients, such as supernova remnants, pulsar wind nebulae, microquasars, and binary systems. VHE $\gamma$-ray telescopes, like Cherenkov telescopes, have enabled the detection of $\gamma$ rays at higher energies than previously possible, revealing a wealth of transient phenomena.

Theoretical models of HE and VHE transients have evolved to incorporate the latest observations and insights. These models include the study of particle acceleration and transport, magnetic field amplification, and radiation mechanisms. Multi-wavelength and multi-messenger observations, including X-rays, radio waves, and neutrinos, are also providing complementary information that helps in the understanding of these phenomena.

In this proceeding, I present recent advancements in the study of HE and VHE transients in the Milky Way and highlighting their importance in the context of high-energy astrophysics. The study of these phenomena promises to deepen our understanding of the universe's most extreme environments.

38th International Cosmic Ray Conference (ICRC2023)
26 July - 3 August, 2023
Nagoya, Japan

*Speaker





PoS(ICRC2023)022

## 1. Introduction

Galactic transient sources is a commonly used expression in the astrophysics community. However, there is no general valid definition of this class of sources. For the purpose of this work, I defined Galactic transient sources in the following way:

- A transient event refers to a sudden and temporary change in the brightness of a celestial object and is characterized by significant changes in the emitting object's properties.
- Unlike variability, transient events are not part of the regular behavior (e.g. Active Galactic Nuclei flares) of the object but are caused by specific and often rare processes or interactions.

Based on this definition the following Galactic source classes were selected for this proceeding: transitional milli-second pulsars, magnetars, supernovae and novae. In the following, the instruments used to obtain the results, presented here, are shortly described before each source class is introduced and presented in more detail.

## 2. Instruments for high and very high energy observations

The study of galactic transient sources requires instruments capable of detecting the most energetic radiation in the universe. By focusing on the high and very high energy regions of the electromagnetic and particle spectra, astrophysicists gain a deeper understanding of the cataclysmic forces and exotic physics governing these celestial outbursts. These instruments, meticulously engineered and operated with precision, open windows into the heart of our galaxy, unveiling the birth and death of stars, the dynamics of compact objects, and the relentless interplay between matter and gravity. In the following, the instruments used in this work for $\gamma$-ray detection at high energies (HE; 100 MeV–100 GeV) and very high energies (VHE, 100 GeV–100 TeV) are listed.

**The Fermi $\gamma$-ray Space Telescope**: Since its launch in 2008, the Fermi $\gamma$-ray Space Telescope has been at the forefront of high-energy astrophysics, revolutionizing our understanding of the universe's most enigmatic and energetic phenomena. The satellite is equipped with two primary instruments: the Large Area Telescope (LAT) and the $\gamma$-ray Burst Monitor (GBM). The LAT can detect $\gamma$ rays with energies ranging from 20 MeV up to more than 300 GeV. It has a large field of view, which allows it to survey the entire sky every three hours. This wide coverage is crucial for detecting transient and variable $\gamma$-ray sources. The $\gamma$-ray Burst Monitor is a complementary instrument on Fermi that specializes in the detection of $\gamma$-ray bursts (GRBs) and other transient events in the $\gamma$-ray spectrum. The GBM covers the energy range from a few keV up to 40 MeV. This makes it suitable for detecting both short and long-duration $\gamma$-ray bursts. For technical details please refer to [1].

**Major Atmospheric Imaging Cherenkov Telescopes - MAGIC**: The two Major Atmospheric Imaging Cherenkov Telescopes, known as MAGIC, are situated on the Canary Island of La Palma, Spain, at the observatory of El Roque de Los Muchachos (28°, 18°W, 2200 m above sea level). These twin telescopes with a dish diameter of 17 m are engineered to capture very-high-energy $\gamma$ rays within an energy range spanning from around 30 GeV to several tens of TeV. For technical details please refer to [2].

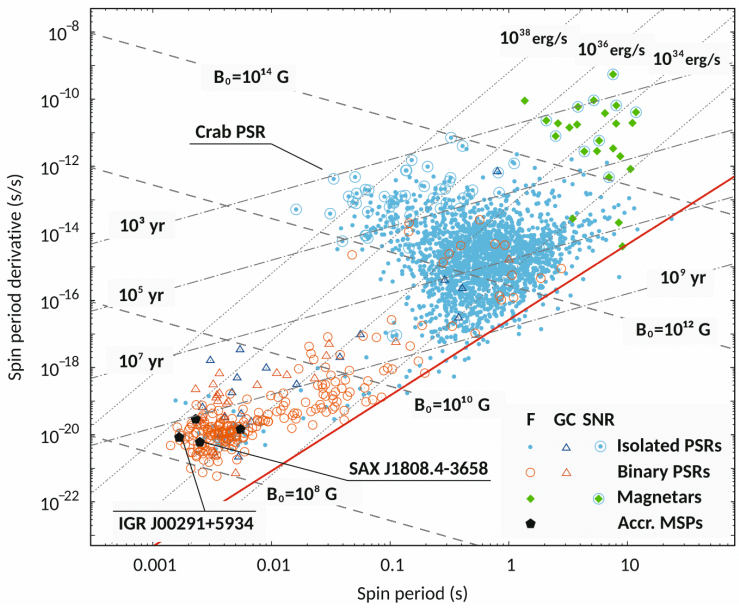


**Figure 1:** $P - \dot{P}$ diagram of rotation-powered pulsars. Symbols mark pulsars found in the Galactic field (F), in globular clusters and supernova remnants. Red solid line: pulsar death line. Figure taken from [7].

**H.E.S.S. (High Energy Stereoscopic System) Telescopes:** The H.E.S.S. telescopes are located in the Khomas Highland of Namibia (23°16′18″S, 16°30′00″E), at an altitude of 1800 m above sea level. In its first phase, the system consisted of four large Cherenkov telescopes each of 12 m diameter. It was then upgraded with a fifth telescope at the center of the array, a single huge dish with a diameter of 28 m. With the full array, H.E.S.S. is sensitive to $\gamma$ rays in the energy range between ∼0.1 TeV and ∼100 TeV. For technical details please refer to [3, 4].

**Very Energetic Radiation Imaging Telescope Array System - VERITAS**: VERITAS is located at the Fred Lawrence Whipple Observatory (31°40′30″N, 110°57′07″W, 1.3 km above sea level), situated on Mount Hopkins in southern Arizona, United States. It is an array of four 12 m optical reflectors sensitive to $\gamma$ rays between 50 GeV and 50 TeV. The system underwent two upgrades by relocating one telescope in 2009 and a camera upgrade in 2012. For technical details please refer to [5].

## 3. Transitional millisecond pulsars

Millisecond Pulsars (MSPs) are a special class of rapidly spinning neutron stars, which are very dense objects of about 1.5 solar masses within a radius of ∼12 km [6]. We define MSPs as having a period shorter than 30 milliseconds, corresponding to a spin frequency exceeding 30 Hertz (Hz). What sets these MSPs apart is their association with binary systems, where they are typically paired with a low-mass companion star weighing less than 1 solar mass ($< 1M_{\odot}$). Additionally, MSPs exhibit relatively weak magnetic fields, typically measuring less than ($< 10^8 - 10^9$ Gauss).

Interestingly, a significant number of these MSP-binary systems are found within the dense environments of Globular Clusters, which are ancient conglomerations of stars. This observation has

led to a fascinating realization: MSPs must be the products of aging systems, allowing ample time for the magnetic fields to transition from their initial high strengths in young neutron star (usually exceeding $10^{12}$ Gauss) to their present, substantially weaker states. Consequently, a compelling hypothesis emerged — the *recycling scenario*.

According to this recycling scenario, older neutron stars are rejuvenated to millisecond spin periods through a process involving the accretion of matter and angular momentum during a phase known as Low-Mass X-ray Binary (LMXB) phase. During this phase, the MSPs gain the necessary momentum to achieve their rapid rotations. Even as their magnetic fields diminish over time, the spin-powered emission mechanism can be rekindled. Therefore, once the accretion phase concludes, often when the companion star has shed its atmosphere or moved away from its Roche lobe, the neutron star emerges as a visible and vigorous rotation-powered MSP.

The evolutionary path can be followed in the "Pulse Period versus Period Derivative diagram" ($P - \dot{P}$ diagram) shown in Figure 1. The evolution goes clockwise starting in the upper left corner (for example, the Crab pulsar) with a high $\dot{P}$, a relatively small $P$ and a high magnetic field marked by the dashed, diagonal lines. The spin-down age ($\tau = P/2\dot{P}$) is shown as dotted-dashed line. The magnetic field within the neutron star behaves akin to a rotating magnetic dipole, emitting radiation in accordance with Larmor's formula. As a result of this magnetic configuration, pulsed emissions are typically observable, particularly in the radio and frequently in the $\gamma$-ray bands. These emissions primarily stem from synchrotron radiation produced by charge currents. These charge currents are generated by electrons and positrons that are ejected from the surface of the neutron star due to the formidable Lorentz force exerted by the magnetic field and the rapid rotation. These charged particles follow intricate trajectories along curved, open magnetic field lines.

This emission process has significant consequences for the neutron star's rotational behavior. As a result of this energy-emitting phenomenon, the neutron star gradually loses rotational energy over time, causing it to decelerate. Assuming the magnetic field remains relatively stable over time, a pulsar traverses horizontally from left to right on the $P-\dot{P}$ diagram along a constant. At some point the magnetic field of the neutron star experiences rapid decay, possibly involving ohmic dissipation and contribution from matter accretion during the subsequent LMXB phase. As a consequence of this magnetic field decline, the pulsar deviates from following a constant magnetic field line and descends towards the lower region of the $P - \dot{P}$ diagram. From there the *recycling scenario* might become active and the pulsar is spun up towards the left lower corner of the diagram becoming a MSP, represented by orange symbols in Figure 1.

Among these MSPs, a unique and dynamic subgroup known as "transitional millisecond pulsars" (tMSPs) has emerged as a focal point of research. TMSPs are characterized by remarkable state changes occurring within a few weeks. These transitions involve a shift from a rotation-powered regime, where the (radio) pulsar wind prevents the infall of matter from the low-mass companion, to an accretion regime where these systems emit intense high-energy radiation akin to X-ray binaries (see Figure 2, right, for a sketch). During these transitions, the luminosity undergoes significant fluctuations, often changing by at least an order of magnitude. These variations are likely attributed to fluctuations in the rate of mass inflow. The discovery of tMSPs stands as a pivotal milestone in the exploration of the evolutionary pathways of MSPs pointing to the *recycling scenario*.

The first direct evidence for such a transition was made in 2013, when the MSP PSR

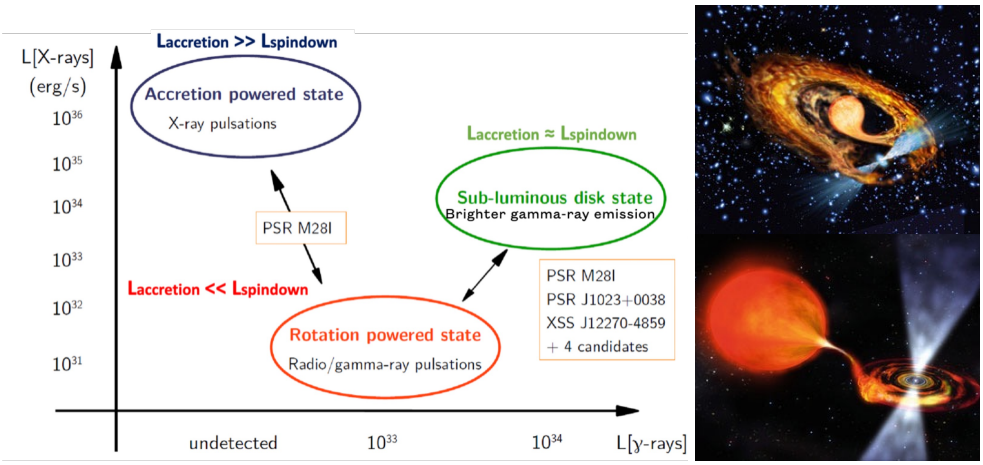


**Figure 2:** *Left:* tMSP states shown in the X-ray versus $\gamma$-ray luminosity diagram. Adapted from [8]. *Right:* Artistic view of the rotation powered state *upper panel* and the accretion powered state (*lower panel*). Figure taken from [7].

J1824–2452I, situated within the globular cluster M28, emitted millisecond X-ray pulsations powered by accretion that was previously known as a rotation-powered radio pulsar [9]. Our knowledge today includes three transitional MSPs that could swing between the two states on timescales of a few days to a few months. These systems have exhibited radio pulsar states (PSR J1023+0038 and PSR J1227–4853) and one of them experienced a significant and luminous accretion outburst (PSR J1824–2452I). However, the most intriguing behavior is their perplexing X-ray sub-luminous disc state, offering a novel perspective on the behavior of LMXBs under conditions of low mass accretion rates. The three states are defined as:

**Radio pulsar state**: The mass inflow rates are sufficiently low, the magnetosphere likely takes precedence and extends up to the light cylinder. Here, the radio pulsar is active, the disc vanishes, and the system emits a dimmer X-ray glow (around $L_X \sim 10^{32}$erg s$^{-1}$).

**Accretion state**: The mass inflow rate is high, the radio pulsar is likely deactivated, and the system shines brightly in X-rays (with $L_X > 10^{36}$ erg s$^{-1}$).

**Sub-luminous disc (accretion) state**: It is characterized by X-ray luminosities $L_X \sim 10^{33}$ erg s$^{-1}$. The systems exhibit variable X-ray fluxes, oscillating between low and high modes, with the majority of their time spent in the latter state, punctuated by occasional flaring events.

See Figure 2, left, for an overview of the states with respect to their X- and $\gamma$-ray luminosities and [7] for an extensive review and references therein.

### 3.1 Transitional millisecond pulsars at high- and very-high energies

During a systematic search for tMSPs at high energies, potential transitional pulsars were identified within the population of binary radio MSPs [10]. These candidates were characterized by donor stars that are presently shedding mass, a phenomenon detected through the irregular eclipses of the radio pulsed emission. These eclipses result from the absorption and scattering of matter expelled from the binary system. The authors searched for GeV in 7 years of *Fermi*-LAT data of 30 tight binaries including two tMSPs known from X-ray observations. Since PSR J1824-2452I

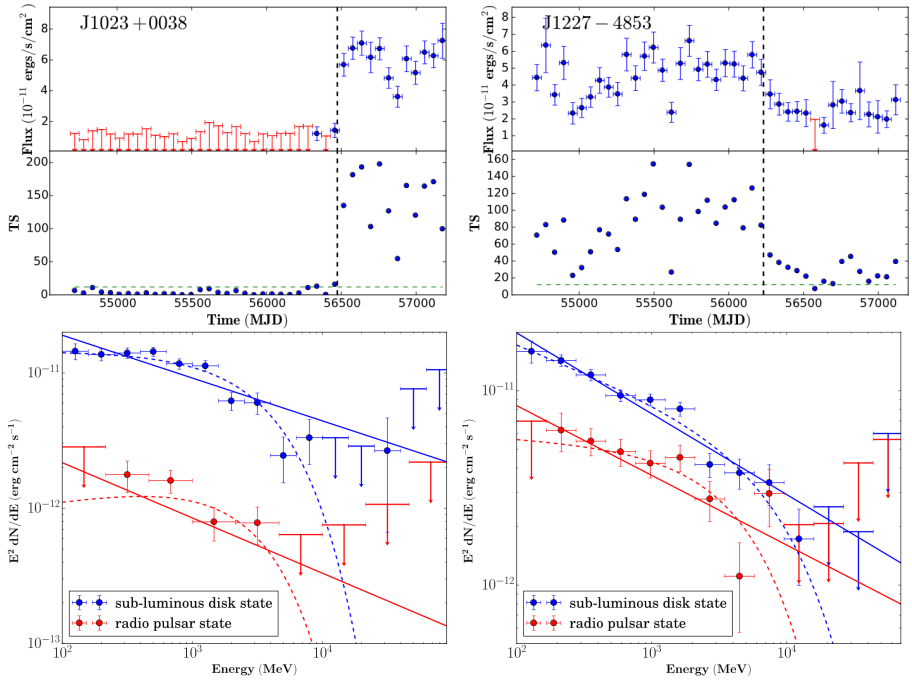


**Figure 3:** *Fermi*-LAT lightcurve and spectrum of J1023+0038 (*left*) and J1227-4853 (*right*). The dotted, vertical line in the upper panels denote the state transition, red arrows show upper limits. In the lower panels the fitted models are shown with solid lines (for a power-law) and dotted lines (for a power-law with exponential cutoff). Figures taken from [10].

is located in a very bright $\gamma$-ray source, the globular cluster M28, the source was excluded from the analysis. Significant flux variations were observed exclusively in the cases of J1023+0038 and J1227-4853, aligning precisely with the previously established state transition times (as depicted in the lightcurves in Figure 3, with the dotted vertical line denoting these transition points).

It is noteworthy that the transitions manifest in opposite directions in synchrony with the changes observed in X-ray and optical flux. While J1023+0038 undergoes a transition from a radio pulsar state (low gamma-ray state) to a sub-luminous disc state (high gamma-ray state), J1227-4853 experiences the reverse shift. Their $\gamma$-ray fluxes during the state transition were observed to fluctuate by a factor ranging from 2 to 5 [10]. Assuming that a similar underlying physical mechanism operates in both sources, the oscillatory nature of this swinging phenomenon is underscored by this observation. The non-detection of transitions in other sources should not be immediately extrapolated to suggest that all tight binary systems, aside from the swinging ones, have definitively completed their swinging phases and are now settled in a final, fully recycled state. Future surveys may potentially reveal a different scenario, which timing and occurrence cannot be predicted with certainty.

The derived spectra show high-energy cutoffs at a few GeV for the high gamma-ray state of PSR J1023+0038 and for both states of PSR J1227–4853 (see Figure 3). Therefore, it is unlikely that the component seen at GeV energies can be seen at TeV energies. Either there is another component appearing at TeV energies or a detection is hard to obtain. However, before that study came out, VERITAS followed the disappearance of pulsed radio emissions from PSR J1023+0038

in June 2013. These observations revealed the emergence of an accretion disk around the neutron star [11]. They searched for both steady and pulsed gamma-ray emissions before and after the state transition, but no significant $\gamma$-ray signals were detected above 100 GeV. By assuming that very high energy gamma rays originate from an inverse Compton mechanism within the shock region, it was deduced that the shock magnetic field must have exceeded approximately $\sim$2 G before the vanishing of the radio pulsar and subsequently increased to at least $\sim$10 G afterward [11].

### 3.2 Transitional millisecond pulsars - Open questions

**What drives variations of the mass in-flow rate?** The transitions between accretion and rotation-powered activity occurring over a span of a few years are commonly ascribed to shifts in the ram pressure imposed by the matter entrapped within the gravitational field of the neutron star. Nevertheless, the underlying factors driving variations in the mass accretion rate remain uncertain. The sub-luminous state may be characterized by an advection-dominated accretion flow, while the brighter accretion state might be explained by a more typical geometrically thin and optically thick disc. However, it has not yet been established whether a disc-like flow can withstand the pulsar wind pressure in the rotation-powered state. An intriguing possibility is the magnetic activity of the secondary star, which may be excited by its rapid orbital-locked rotation. This magnetic activity could potentially drive surges in the mass transfer rate, necessary to compress the pulsar wind and initiate the formation of an accretion disc.

**What is the origin of the gamma-ray emission during the intermediate accretion stage?** There are models where a substantial portion of the matter in the disk is propelled away and these models have proven effective in explaining $\gamma$-ray emissions. The emission arises from self-synchrotron Compton processes occurring at the turbulent interface between a propelling magnetosphere and the inflowing disk. Recent detections of optical pulses suggest the presence of an active rotation-powered pulsar. Nonetheless, it remains uncertain whether these optical pulses originate in a magnetospheric environment (as seen in other MSPs) or potentially result from a miniature pulsar wind nebula.

**Are all millisecond pulsars in close binary systems transitional?** Intensive efforts are currently underway to uncover new systems associated with gamma-ray sources, displaying distinctive X-ray and optical behaviors. Concurrently, continuous monitoring of tight binary systems is poised to expand the list of confirmed tMSPs. This expansion is crucial for determining whether all MSPs in tightly-bound binary systems have the potential to transition or if additional factors, such as the magnetic activity of the secondary star or the magnetic dipole inclination of the neutron star, are prerequisites for triggering state transitions. Expanding this sample size will allow population studies of MSP binaries with short orbital periods, moving beyond the current case-by-case approach.

**What is a good observation strategy to hunt for tMSPs at TeV energies?** Although the spectral cutoffs at GeV energies do not look promising regarding the detection of TeV emission, we cannot exclude another component generated farther away than the surroundings of the binary system. The best strategy to identify candidates has been actually to look for distinctive variability in the optical and X-ray band and compare their location with the spatial error bars of unidentified *Fermi*-LAT sources.

Please see [7] as source for this chapter and for an extensive review about MSPs and tMSPs.

## 4. Magnetars

Magnetars represent a distinct class of intensely magnetized neutron stars, exhibiting a diverse range of X-ray phenomena. These include short bursts, outbursts, sudden and dramatic alterations in pulse profiles, quasi-periodic oscillations and various timing irregularities such as heightened spin-down rates. The population of identified magnetars consists approximately of 30 objects[1]. Until 2010, they population was located in the upper right corner of the $P - \dot{P}$ diagram showing a surface magnetic field (as inferred from the spin-down rate) higher than the electron critical field $\simeq 4.4 \times 10^{13}$ G, (green markers in Figure 1). However, by extending the population is was found that magnetars can also behave like so-called 'conventional' X-ray and radio pulsars exhibiting magnetar-like behavior occupying unexpected low magnetic field regions within the $P-\dot{P}$ diagram (See review and references within [12]). Despite their low dipolar field, they maintain a substantial internal toroidal field of approximately $10^{14}$ G capable of sporadically triggering crustal displacements, resulting in the twisting of the external magnetosphere, as well as the generation of potent magnetospheric currents that cause episodes of bursting activity. The authors of [13] even suggest to call the magentar-like phenomena as 'magnetic restlessness' in neutron stars instead of classify these objects as 'magnetars'. Nevertheless, the bursting activities seen in the soft and hard X-ray can be classified into:

**Short bursts**: The sudden release of X-ray and gamma-ray photons persists for durations ranging from milliseconds to a few seconds, with peak luminosities typically falling within the range of approximately $10^{36}$ to $10^{43}$ erg/s. These bursts commonly exhibit a single-peaked and asymmetric profile, characterized by a swifter rise than decay. While instances of two or multi-peak bursts do occur, the rapid succession of burst events can blur the distinction between the peaks. Certain bursts, typically the most luminous ones ('intermediate flares'), can be succeeded by X-ray tails that last from minutes to hours. The spectral emission can be usually modeled well by a single- or a double-black-body model.

**Outbursts**: In the context of magnetars, 'outbursts' refer to a substantial amplification (~10 to 1000) in flux that gradually diminishes over a span of several months or, in some cases, years. Particularly, their initial stages are typically linked to one or more short bursts. The changes in flux occur swiftly and often within a span of approximately 1 to 2 days. The decay often commences with an initial rapid decline (around 1 day) followed by a more prolonged period that can be characterized by power-law or exponential functions. During the initial stages of the outburst, the X-ray spectrum tends to be more energetic compared to the quiescent phase, and it gradually becomes less intense as the flux diminishes. Interestingly, outbursts are frequently accompanied by alterations in the timing characteristics of the magnetar.

**Giant flares**: Giant flares represent the most infrequent and incredible energetic events linked to magnetars. To date, a total of three giant flares have been documented, and a fourth one, which will be discussed in the following section, was recently detected. These occurrences include events in 1979 from SGR 0526–66, on August 27, 1998, from SGR 1900+14, and on December 27, 2004, from SGR 1806–20. All three giant flares commenced with a brief burst of hard X-rays, lasting ~ 0.1 – 0.2 seconds, and exhibiting peak luminosities in the range of $10^{44}$ to $10^{45}$ ergs per second. The spectrum of this sudden burst of radiation extends to at least the MeV range and can be characterized

[1] https://www.physics.mcgill.ca/~pulsar/magnetar/main.html

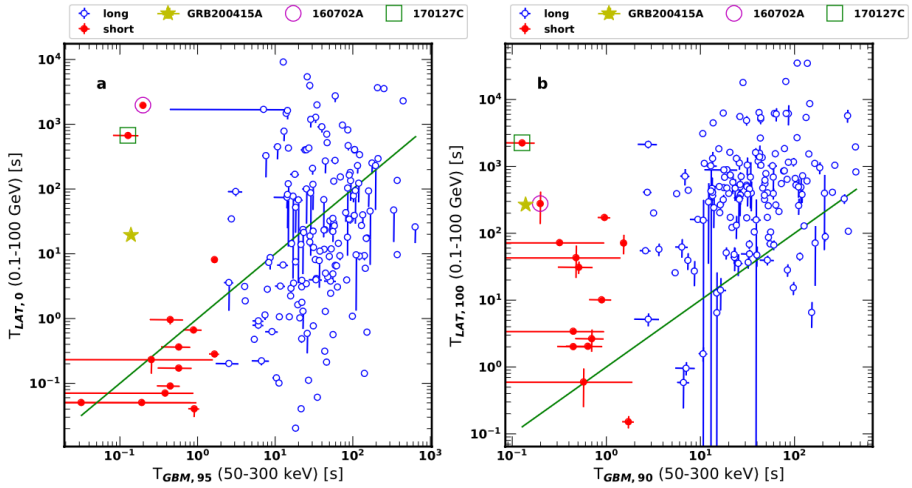


**Figure 4:** Comparison of GRB 200415A (marked as yellow star) with short (red, filled circles) and long (blue, open circles) GRBs from the second *Fermi*-LAT GrB catalogue. *Left:* Onset times detected by the *Fermi*-LAT versus the end of the GRB detected by the GBM. *Right:* Durations in the 100 MeV–100 GeV energy range versus durations in the 50–300 keV energy range. Two sGRBs with similar durations are marked with a magenta circle and green square. Figure taken from [16].

as a black body spectrum, with initial temperatures ranging from ~ 30 – 200 keV (for SGR 0526–66 and SGR 1806–20, respectively). These extraordinary releases of energy had measurable effects on Earth's magnetic field and ionosphere. Subsequent to the initial spikes, afterglows emerged that exhibited clear modulation at the rotational period of the neutron stars. These afterglows were notably softer than the initial burst and gradually softened and faded over the course of several minutes. Quasi-periodic oscillations were detected in the tails of the three giant flares and started the field of asteroseismology of neutron stars.

For extensive reviews on magnetars and sources for this section see [13, 14].

### 4.1 Magnetars - Giant flares at high energies

On April 15, 2020, a significant event occurred — the fourth-ever detected giant flare from a magnetar. What makes this event even more extraordinary is that it marked the first occurrence of such a phenomenon at MeV and GeV energy levels. *Fermi*-GBM was the first instrument triggered by the event that was initially categorized as a short gamma-ray burst (sGRB) GRB 200415A, associated with the galaxy NGC 253 (the Sculptor galaxy), an active star-bursting intermediate spiral galaxy at a distance of ~3.5 Mpc. This association together with the similarity to the GBM sub-MeV light curve of the previously identified extragalactic soft gamma repeater giant flare candidates GRB 051103 and GRB 070201, as well as the detection of quasi-periodic oscillations by the Atmosphere–Space Interaction Monitor, led to the classification of GRB 200415A as a magnetar giant flare (MGF) located in the Sculptor constellation ([15] and references therein). The *Fermi*-LAT detected three events associated with high probability of >90% with the MGF event. These events had arrival times after $T_0$ of 19 s, 180 s and 284 s and energies of 480 MeV, 1.3 GeV and 1.7 GeV, respectively [16]. The derived spectrum does not look different from spectra of other sGRBs detected with the *Fermi*-LAT. The difference lies in the long time delay between the GBM

trigger time and the detection by the *Fermi*-LAT. The typical value is less than 1 s, while the delay time for GRB 200415A was 19 s. This is illustrated in the left-hand plot of Figure 4, where data taken from the second LAT GRB catalogue (2FLGC) are shown. The timing of the first arrival of a high-energy LAT $\gamma$-ray with a probability of >0.9 associated with the GRB can be seen. This timing signifies the initiation of high-energy emissions. It is presented in relation to the GBM T 95, which denotes the conclusion of the prompt emission recorded by the GBM. In the case of the short burst GRB 200415A, there is a notably extended delay in the onset of the high-energy emissions compared to the conclusion of the prompt phase. This delay in high-energy emission onset is observed in only two other short bursts within the 2FLGC dataset.

The authors of [16] propose that an ultra-relativistic outflow collided with a dense shell of material surrounding the magenetar. Electrons accelerated in the shock-heated material can reach relativistic speeds, resulting in synchrotron radiation within the magnetic field generated by the shocks. Consequently, the high-energy component of the spectrum of an MGF is represented by GRB 200415A leading to the conclusion that magnetars might be capable of powering some short $\gamma$-ray bursts.

#### 4.1.1 Magnetars - Fast radio bursts

Fast Radio Bursts (FRBs) are transient radio pulses of milli-second duration with unknown cosmic origin. They were discovered in 2007 and fill now a catalog[2] of almost 1000 sources, 19 of them with confirmed host galaxies[3] (z~0.034 – 0.66). Characteristic for FRBs are their relatively broad-band pulses showing quite large dispersion delays, which point to extra-galactic origin. [17] tried to find counterparts for FRBs to shed light on the their origin. They searched for spatial correlations between FRBs and gamma-ray bursts, but could not find any significant result. More details and references can be found in [18, 19].

No counterpart or progenitor to radio emission was detected until on April 28, 2020, when the radio instrument CHIME detected an FRB in spatial coincidence the magnetar SGR 1935+2154 [20]. The burst had a double-peak structure with two components ~5 ms wide separated by ~30 ms (see Figure 5). Apart from the radio detections, SGR 1935+2154 experienced a storm of X-ray bursts that lasted for several hours. This activity was detected by various X-ray telescopes, including NICER, Chandra, XMM, NuSTAR, and Swift XRT and BAT, as well as the gamma-ray telescopes Fermi and Integral. Notably, the X-ray peaks lagged behind the radio peaks by 6.5 milliseconds. This event made SGR 1935+2154 the first FRB in the Galaxy and the first identified FRB source and supported the long-standing hypothesis of a magnetar-FRB association. However, observationally, most of the hard X-ray bursts from SGR 1935+2154 were not accompanied by FRBs. This aligns with the understanding that FRB emissions, particularly those generated by magnetars, are narrowly beamed rendering the associations between FRBs and SGR bursts rather uncommon [22].

SGR 1935+2154 is located at 6.6 kpc with a spin period of 3.24 sec. It is hosted by an evolved SNR (G57.2+0.8), which likely interacts with a surrounding molecular cloud [23]. There exist several models for the emission side summarized in [24]. These models can be categorized into two groups: the ones that involve the magnetospheres of a compact object (most likely a neutron star)

[2] https://www.wis-tns.org/
[3] https://www.frb-hosts.org/

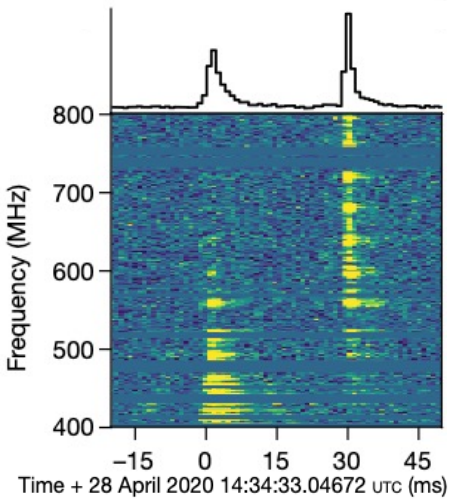


**Figure 5:** Total intensity normalized dynamic spectrum and band-averaged time-series of the detection by CHIME/FRB. Dynamic spectra are displayed at 0.98304-ms and 1.5625-MHz resolution. The bursts detected by CHIME/FRB exhibit a 'comb-like' spectral structure. This pattern results from their detection in a beam sidelobe and from dispersed spectral leakage, which is attributed to instrumental factors. Figure taken from [21].

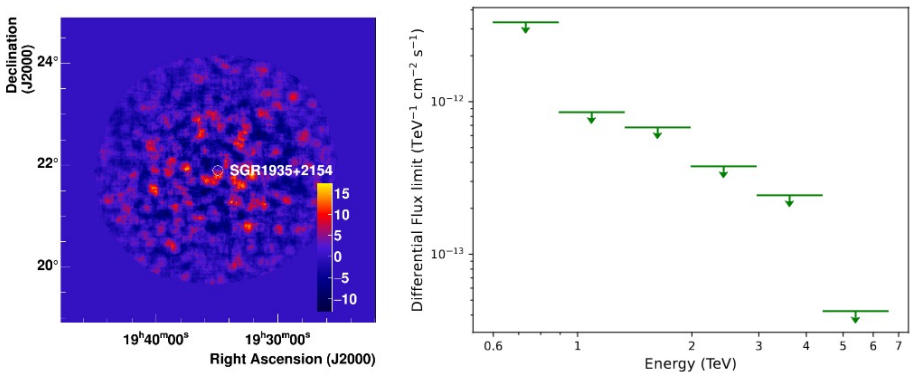


**Figure 6:** *Left:* Excess map computed by H.E.S.S. on SGR 1935+2154. *Right:* Differential 95% C.L. upper limits calculated from H.E.S.S. observations on SGR 1935+2154. Figure taken from [29].

and those that involve relativistic shocks occurring far outside the magnetospheres interacting with the surrounding ISM. The former can be referred to as 'pulsar-like' models, while the latter can be termed 'GRB-like' models. Regarding TeV emission, there are also several model predicting it [25–27].

During the X-ray bursts from SGR 1935+2154, MAGIC could not observe due to the pandemic lockdown. However, multi-wavelength campaigns were done without any significant detection [28]. The H.E.S.S. transients follow-up system initiated Target of Opportunity observations on SGR 1935+2154 following a Swift-BAT alert. Due to darkness and visibility constraints, follow-up observations could not begin until about 7.5 hours later resulting in upper limits. (see Figure 6) [29]. The absence of VHE $\gamma$ rays aligns with predictions for typical magnetar bursts (not the giant flares) when a thermal emission mechanism is at play [30].

### 4.1.2 Open questions

**How is FRB emission generated?** This question is connected to the question whether FRBs emit TeV $\gamma$ rays. Their non-detection might be connected to the location of the $\gamma$-ray emission. If the emission occurs very close to the magnetar's surface, pair production and photon splitting cause substantial energy losses for VHE $\gamma$ rays. This results in significant cutoffs in the MeV to GeV energy range. On the other hand, if the emission is caused by a GRB-like mechanism, the $\gamma$ rays are generated well away from the magnetar's intense magnetic field and might be detectable by Cherenkov instruments. Future observation might shed light on this question.

## 5. Supernovae

Supernovae (SNe) are powerful explosions that occur when massive stars reach the final stage of their evolution. They are usually classified in SN Ia and core-collapse (cc-)SNe (type II, and type Ib/c). Detectable $\gamma$-ray emission is expected rather from Type II SNe due to the strong wind of the progenitors providing a very dense environment. Furthermore, cc-SNe, occurring in a dense circumstellar medium (CSM) are possible candidates for accelerating Cosmic Rays (CRs) to PeV energies. Here, Type IIn are preferred candidates due to their spectral features, which are indicative of CSM interaction (e.g.[33–36]).

Models predict that within a few days of a SN shock propagating through a very dense CSM, a collision-less shock can form. The high shock velocity and the ionized state of the CSM enable particle acceleration, which drives the growth of plasma instabilities. These instabilities, in turn, facilitate further particle acceleration. This iterative process results in the rapid and significant amplification of the magnetic field. Such a high magnetic field is essential for accelerating particles to very high energies (e.g.[37, 38]). [39] found the sources SN 1986J (SN IIn) and SN 1993J (SN IIb) to be the most efficient at generating turbulent magnetic fields and accelerating CRs. They estimate that the CRs reach maximum energies of ∼1–10 PeV within a few days after the explosion and ∼0.1–1 PeV after one year. Therefore, TeV $\gamma$-ray emission should be detectable weeks after such outbursts. Figure 7, left, sketches the environment of CR acceleration in SNe: the dense CSM is generated by the progenitor wind, which exhibits a high mass-loss rate combined with a low wind velocity.

### 5.1 The case of SN 1987A

The most recent extra-galactic, unaided eye SN was the type II SN 1987A located in the Large Magellanic Cloud [40]. X-ray observations suggest that the blast wave has swept up the equatorial ring - the densest region in the immediate circumstellar environment. Based on Diffuse Shock Acceleration (DSA) models, in such a case one would expect TeV $\gamma$-ray emission from CR protons accelerated in the shock. The emission should be variable due to changing CSM density and acceleration timescales. Despite the fact that the TeV emission is already past its maximal brightness of $\sim 10^{-13}$erg cm$^{-2}$ s$^{-1}$, the current levels should still be detectable with sensitive instruments like H.E.S.S. [41, 42]. Up to now, neither the *Fermi*-LAT nor the H.E.S.S telescopes $\gamma$-ray could detect emission from the source [43, 44]. However, [45] found a hint of rising GeV emission from the SN 1987A region in *Fermi*-LAT data. The increase is seen only at >1 GeV energies and indeed

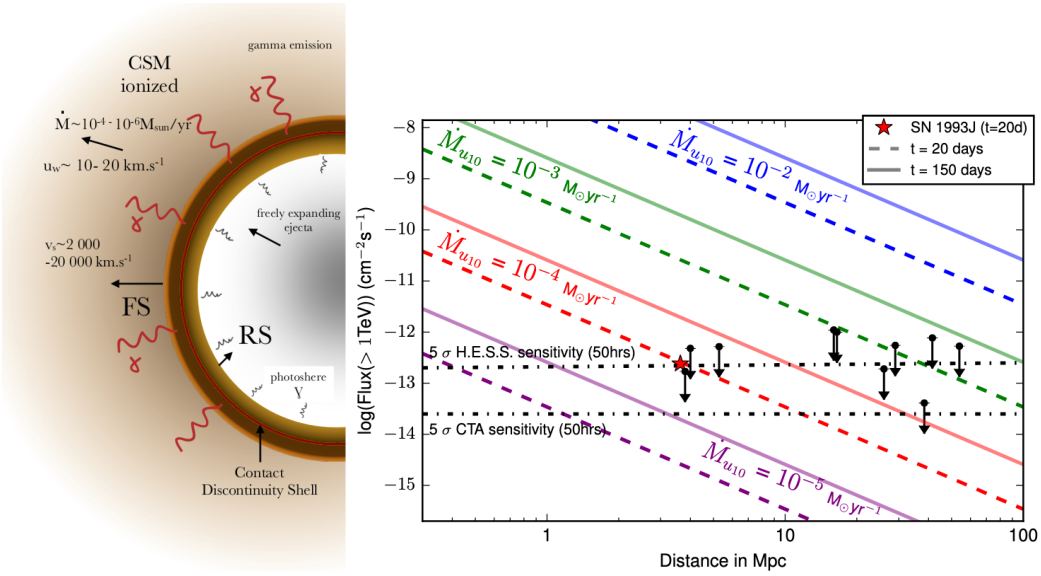


**Figure 7:** *Left:* Sketch of the $\gamma$-ray emission at a supernova shock front with typical Type IIP values for shock velocity, pre-outburst mass loss rate, and wind velocity. *Right:* Predicted Flux(>1 TeV) as a function of the distance to the source. Figures taken from [31] and [32].

comparable to predictions by DSA models. Since there is no clear variability detected in X-rays, it might hint at hadronic emission from SN 1987A. Still, the source region is crowded and the poor localization allows several other counterparts for the detected emission. More sensitive future instruments, like the Cherenkov Telescope Array Observatory (CTAO), might help to resolve the emission region.

### 5.2 Core-collapse SNe searches

The H.E.S.S. collaboration performed a systematical search for $\gamma$-ray emission from ten cc-SNe in nearby galaxies within a year following the corresponding SN event [46]. No significant $\gamma$-ray emission has been detected from any of the objects. Upper limits on the $\gamma$-ray flux above 1 TeV have been established at approximately $10^{-13}$ cm$^{-2}$s$^{-1}$, which corresponds to luminosity upper limits in the range of about $2 \times 10^{39}$ to $1 \times 10^{42}$ erg s$^{-1}$. Using the model of [47] for hadronic $\gamma$-ray emission from young supernova remnants, the authors constrained the CSM density around the SNe. The corresponding upper limits on the mass-loss rates span from $\sim 2.5 \times 10^{-5}$M$_\odot$yr$^{-1}$ up to $\sim 1.6 \times 10^{-3}$ M$_\odot$yr$^{-1}$, which is consistent with predicted mass-loss rates for type IIP SN progenitors. This non detection at VHE and also at HE [48] does not necessarily exclude CR acceleration by SNe. Instead, the CSM densities might have simply been too low for generating $\gamma$-ray emission at a detectable level or that the selection of possible emitters was not optimal. However, there are potential detections of the sources SN iPTF14hls and SN 2004dj (SN IIP) [49, 50]. A transient $\gamma$-ray signal could be tentatively associated with the former source, though it might be confused with a quasar within the field of view. For the second case, a fading GeV $\gamma$ ray source is spatially coincidence with SN 2004dj, however, the chance coincidence is just 0.2%.

In May 2023, the closest (~6.4 Mpc within M101) core-collapse (type II, possible II-L) SN in the northern hemisphere in the last few decades occurred: SN2023ixf [51]. It is the second brightest

SN (mag = 14.9) among all-type SNe after the discovery of SN 1987A in optical bands [52]. The source was detected at X-rays, but neither at HE nor any detection reported at VHE [53, 54].

### 5.3 Type Ia and super luminous SNe

Although type II SNe are theoretically the best candidates to emit $\gamma$ rays due to the strong wind of the progenitors, [55] followed up the type Ia SN 2014J with the MAGIC telescopes to probe a possible production of VHE $\gamma$ rays during the first days after the explosion. The SN is located in the starburst galaxy M 82 at a distance of 3.6. Mpc making it the nearest Type Ia SN within the last decades. The source could not be detected, but an expected emission from the source region was derived by applying the model from [47] for hadronic $\gamma$-ray emission. The resulting SN density profile and a constant density medium resulted in a flux of $\approx 10^{-24}$ photons cm$^{-2}$ s$^{-1}$. An increase of the flux is not expected in the near future, suggesting that the source is undetectable even for the next generation of Cherenkov telescopes like CTAO.

Super luminous supernovae (SLSNe) have also been studied as possible $\gamma$-ray emitters. They have luminosities $\sim$10 – 100 times greater than ordinary core-collapse SNe. Furthermore, an additional power source from standard SNe Types I and II might be present: injection from a rapidly spinning magnetar (see [56] and references within). In this scenario high-energy $\gamma$-rays generated in the magnetar's wind nebula could escape through the expanding SN ejecta at later stages, months or more after the optical peak [57]. Observations with the *Fermi*-LAT and VERITAS of two Type I SLSNe, SN2015bn and SN2017egm, were performed. None of the potential sources were detected and predictions for the Type I SLSNe rate for VERITAS and CTAO were estimated. Considering observation constraints and the time delay due to the optical depth, for sufficiently nearby and bright SLSN-I, VERITAS should be able to observe 0.4 and 4 SLSNe per year from 10 and 50 hours of observation, respectively. Similarly, CTAO is expected to observe 8 and 80 explosions per year under the same conditions.

### 5.4 Predictions & Open questions

The upper limits derived after the search for $\gamma$-ray emission from ten cc-SNe mentioned in section 5.2, were used to display the computed $\gamma$-ray flux as a function of the distance for different values of the pre-SN mass-loss rate, together with the typical five sigma point-source sensitivities of H.E.S.S. and CTAO (see Figure 7). According to the figure, a type IIP SN with a mass-loss rate of $10^{-4}$ M$_\odot$yr$^{-1}$, occurring at a distance of 10 Mpc, should be detectable with H.E.S.S. 20 days after the outburst. CTAO could detect a type IIP SN with the same mass-loss rate occurring at 30 Mpc. However, it has to be kept in mind that SNe with such a dense CSM may not be common. [46] predicts that among all types, SNe with a mass-loss rate above $10^{-4}$ M$_\odot$yr$^{-1}$ should occur within a radius of 10 Mpc at a rate of one per year.

**What to expect at very high energies?** The works by [58] and [59] show theoretical predictions. [58] estimated the $\gamma$-ray signal from typical Type II-P cc-SNe in the first month after the SN explosion considering non-isotropic time-dependent attenuation due to pair production. The $\gamma$-ray emission becomes similar to the unabsorbed solution after a few tens of days. The authors find that the $\gamma$-ray signal from typical extragalactic cc-SNe located at 1 Mpc is undetectable for Cherenkov telescopes after inclusion of the two-photon annihilation process. Therefore, only nearby Type II-P

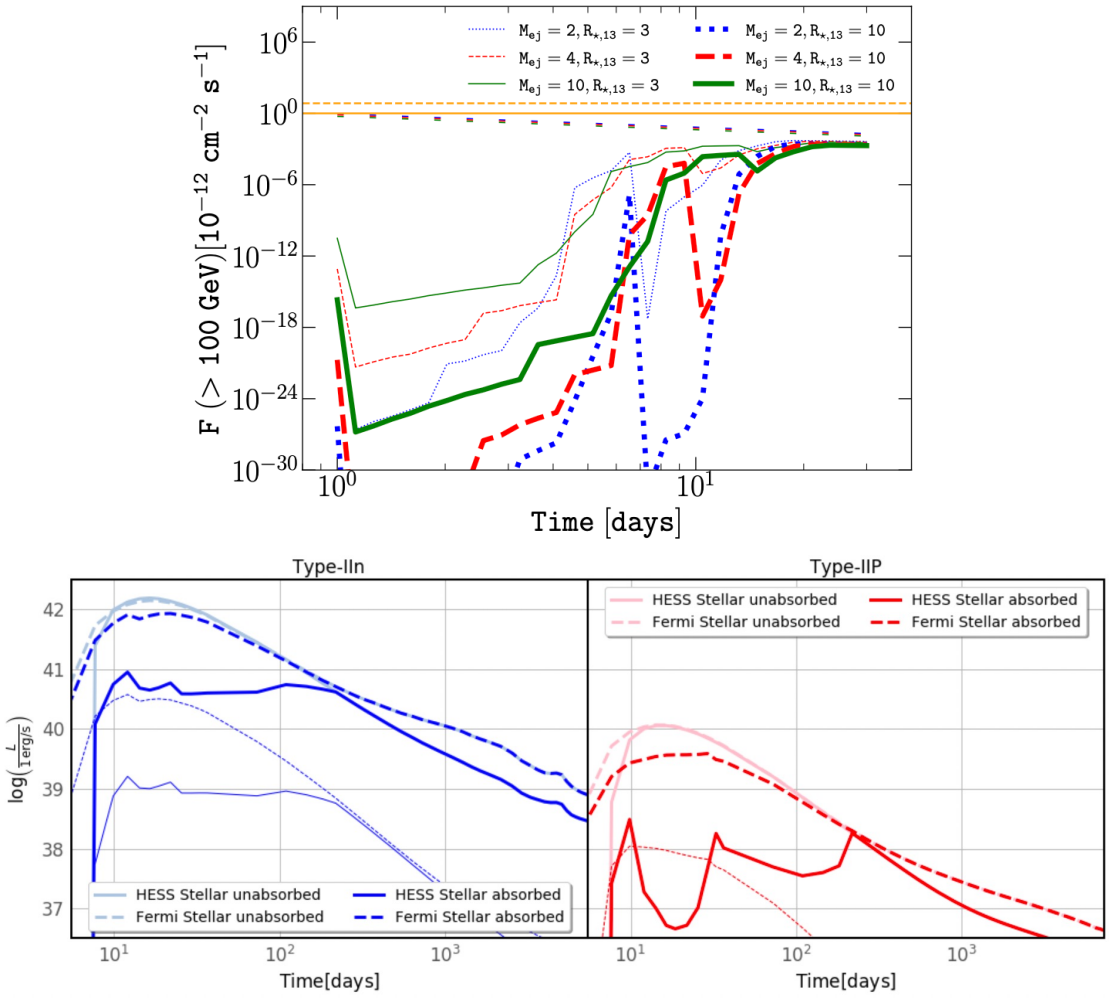


**Figure 8:** *Top:* Time evolution of the integrated photon flux >100 GeV. Source distance: D = 1 Mpc, mass-loss rate of the red supergiant wind: $\dot{M}_w = 10^6\ M_\odot yr^{-1}$. Results for different ejecta masses $M_{ej}$ and progenitor radii $R_\star$ are shown. The corresponding unattenuated fluxes are shown as loosely dotted lines. CTAO sensitivities for 50 h and 2 h are represented by the solid and dashed orange horizontal lines, respectively. *Bottom:* $\gamma$-ray luminosities in the *Fermi*-LAT energy range (dashed) and H.E.S.S. energy range (solid) for the stellar ambient field accounting for $\gamma\gamma$-absorption (strong colors) and without absorption (pastel colors). Thick lines: high mass-loss cases; thin lines: moderate cases. Middle peaks visible in predicted absorbed H.E.S.S. light curved is the numeric artifact. Figures taken from [58] and [59].

SNe, which typically explode in our Galaxy or in the Magellanic Clouds, might be detectable by future instruments like CTAO. Furthermore, such Type II-P SNe generally interact with a relatively diluted medium. SN types evolving in a higher-density medium (such as some Type IIb and IIn SNe) would probably improve chances of a VHE detection. Figure 8 illustrates the $\gamma$-ray signal taking into account the changing temperature and luminosity of the photosphere. An increase of these parameters leads to an enhancement of the attenuation. Changes by a factor of $\sim 2-3$ on some parameters like the stellar radius, and thus on the expected temperature, can lead to dramatic changes in the level of absorption. Finally, the largest $\gamma$-ray fluxes from Type II-P cc-SNe in the first

days after the SN explosion are expected when the mass-loss rate and the ejecta mass are the highest and the total explosion energy and the stellar radius are the smallest. Under these circumstances the sources could potentially be detected by next generation instruments, like CTAO.

The acceleration of CRs in SNe expanding into dense environments around massive stars was studied using numerical simulations by [59]. Taking into account the strong $\gamma\ \gamma$ absorption in the first days after explosion, the authors tested typical CSM parameters for freely expanding winds expected around red supergiants and luminous blue variables stars. They constrained the maximum achievable particle energy to <600 TeV, even for the highest magnetic fields and mass-loss rates. These energies are reached in the presence of a strong stellar field from the progenitor star, which could be sufficient to explain the proton CR spectrum up to the knee at 700 TeV.

Figure 8 illustrates the evolution of the $\gamma$-ray luminosity for different energy ranges. The intrinsic $\gamma$-ray luminosity is significantly reduced by $\gamma\ \gamma$-absorption due to the SN photosphere. 12–30 days after the explosion the intrinsic peak luminosity is reached, because of the time needed to accelerate enough particles to the relevant energies. In the light curve of Type-IIP SNe a second peak is visible resulting from the rapidly fading photosphere after strong $\gamma\ \gamma$-absorption effects. The $\gamma$-ray peak-luminosities are consistent with present upper limits. Current-generation instruments should be able to detect $\gamma$-ray emission from Type-IIP explosions at distances up to $\approx$ 60 kpc and Type-IIn explosions up to $\approx$ 1.0 Mpc.

In summary, the detection of SNe with future instruments like CTAO should be feasible. However, the explosion needs to occur within our galaxy or at most in the Magellanic Clouds to be detectable.

## 6. Novae

Novae occur in close binary star systems consisting of a white dwarf (WD) and a companion star, usually a main-sequence star, Red Giant, or another white dwarf. As the hydrogen pulled from the companion star onto the WD accumulates, a thermonuclear runaway reaction can be triggered. This explosive fusion of hydrogen into helium releases a vast amount of energy resulting in a sudden and dramatic increase in the brightness of the white dwarf. Unlike SNe, novae do not destroy the white dwarf, and the process can repeat (recurrent novae). If the white dwarf's companion is a main-sequence star, the event is referred to as a classical nova. Conversely, if the companion is a Red Giant, the nova is termed symbiotic, which is a rare occurrence. The recurrence interval of nova explosions is believed to be influenced by the white dwarf's mass and the rate of accretion. For a complete review please refer to [60].

### 6.1 Novae in the high-energy range

Since long time it was assumed that particle acceleration (protons or electrons) via shock acceleration can occur in the dense wind of the Red Giant due to the enhanced magnetic fields in the surrounding (e.g. [61]). Finally, on March 10, 2010, the first nova at GeV energies was detected with the *Fermi*-LAT: V407 Cyg. It was visible at high energies the same day as the discovery in the optical (see [62] and references therein). The $\gamma$-ray flux peaked 3 – 4 days after the initial $\gamma$-ray detection. The activity spanned a total of two weeks. VERITAS followed up on the source on the days 9 – 16, but could not detect it. However, the derived upper limits put constraints on hadronic

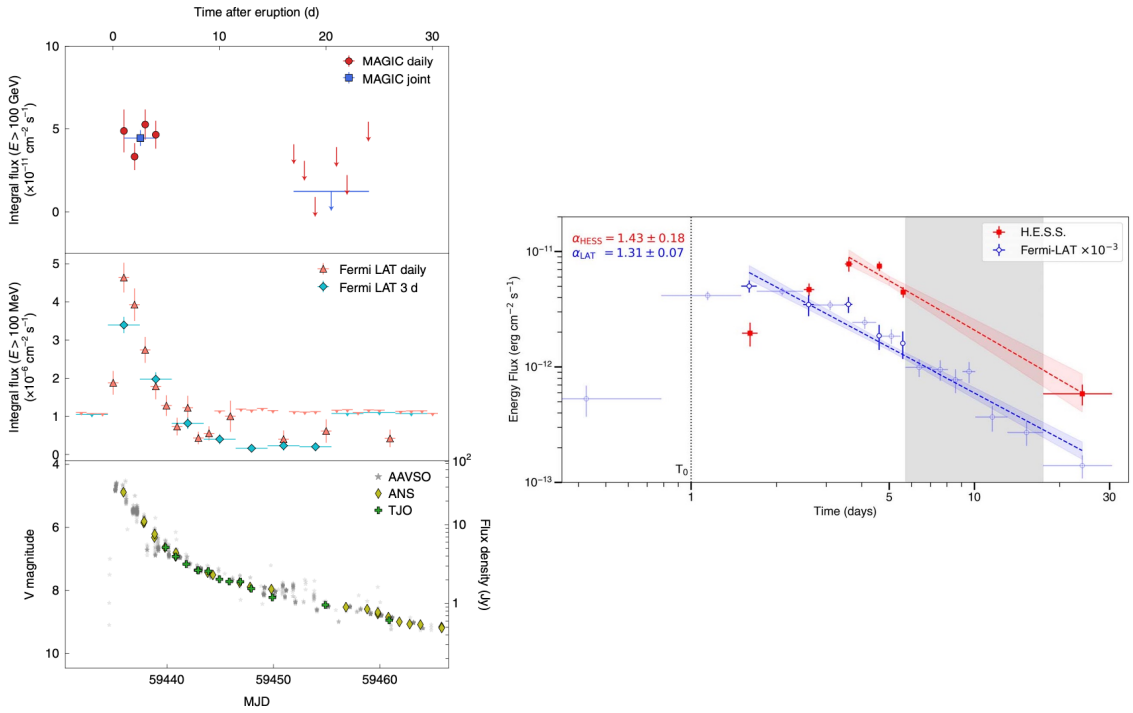


**Figure 9:** *Left:* Light curves in the VHE range (MAGIC, top), HE range (*Fermi*-LAT, middle) and optical (TJO, ANS and AAVSO). MAGIC could not observe continuously between MJD 59440 and MJD 59454 due to bad weather and strong moonlight. *Right:* Light curves from H.E.S.S. and *Fermi*-LAT. Shaded area: moon break for H.E.S.S. observations. Figures taken from [66] and [67].

model parameters [63]. Since then around 20 novae were detected with *Fermi*-LAT[4] and some general properties can be derived from this population. The duration of activity is around 5 – 55 days with rise and fall times of 2 – 7 days. The flux maximum (>0.1 GeV) is around $0.1 - 5 \times 10^{-6}$ ph cm$^{-2}$ s$^{-1}$ and the spectra follow a power-law with indices between 1.8 – 2.3, though many show cutoffs in the GeV range [64]. The average luminosities (>0.1 GeV) are around $10^{34} - 4 \times 10^{36}$ erg s$^{-1}$ [60]. A catalogue with distances of 402 Galactic novae was compiled by [69]. The author calculated distances using Gaia DR3 parallaxes and other auxiliary methods. Two populations could be found: ∼40% located in the Galactic Bulge (D ∼ 8.0 ± 0.8 kpc) and the rest in the Galactic Disk (scale height 140 ± 10 pc). Looking at the *Fermi*-LAT GeV Novae population with 19 detections between 2008 – 2023, the majority of 15 are in the Galactic Disk and 4 in the Galactic Bulge. The ones in the Galactic Disk tend to be closer and brighter: 13 out of the 17 were the optically brightest novae. On average, there are ∼ 1.3 *Fermi*-LAT detections every year steadily increasing the novae population at GeV energies.

### 6.2 Novae in the very-high-energy range

Since high energy data alone are not enough to disentangle electron and proton acceleration models, Cherenkov telescopes had searched for a VHE component in novae for more than a decade without any detection [63, 65]. Nonetheless, models predict acceleration of particles in the nova

[4] https://asd.gsfc.nasa.gov/Koji.Mukai/novae/latnovae.html

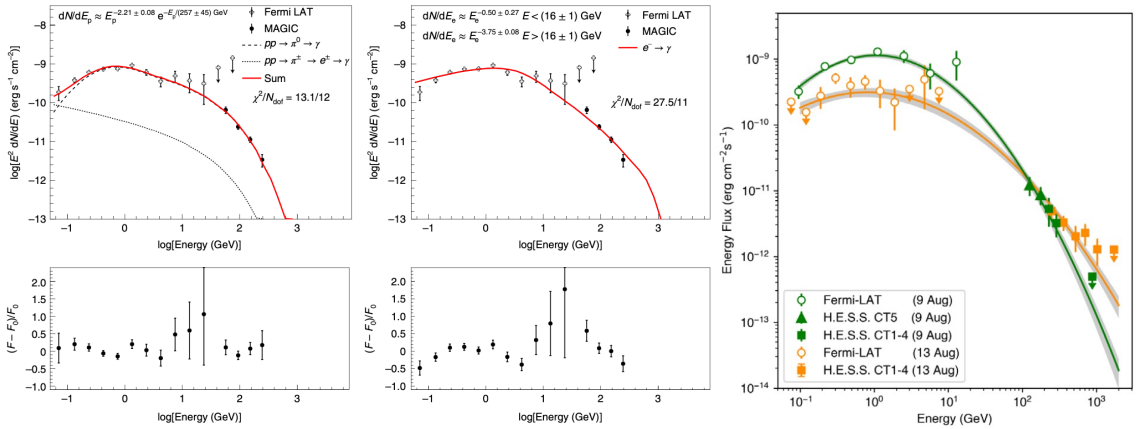


**Figure 10:** *Left and middle:* RS Ophiuchi $\gamma$-ray spectrum measured by *Fermi*-LAT and MAGIC over the first 4 days of the outburst. Modelled with a hadronic (left) and a leptonic (middle) model. Fit residuals are shown at the bottom. *Right:* Spectra measured by *Fermi*-LAT and H.E.S.S. for two different days fitted with a log-parabola model. Figures taken from [66] and [67].

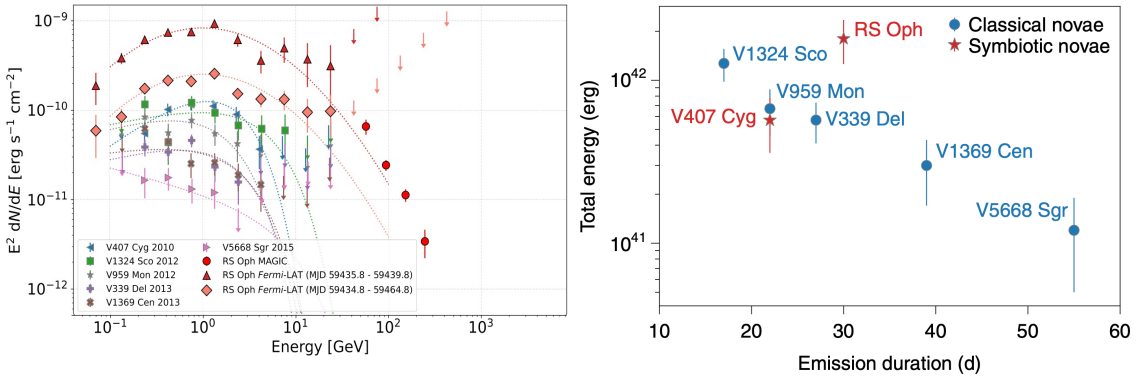


**Figure 11:** *Left:* Comparison of the spectrum from RS Ophiuchi with spectra of other *Fermi*-LAT-detected novae. *Right:* Total energy versus the duration of the RS Ophiuchi outburst compared to other novae detected with the *Fermi*-LAT. Figures taken from [67].

shock through non-thermal processes. Protons can reach much higher energies due to lower energy losses and thus possibly produce a second component detectable by Cherenkov Telescopes. The well-known binary system RS Ophiuchi displaying major outbursts every $\sim$ 15 years as a recurrent symbiotic nova, had its latest outburst in August 2021 and was detected in the VHE range by H.E.S.S., MAGIC, and LST-1 (the first Large-sized Telescope of the CTAO) [66–68]. These detections established novae as new source class at VHE $\gamma$ rays. The observations started around one day after the optical and GeV detection [70, 71]. As shown in Figure 9, the optical and GeV emission peak almost at the same time. The GeV emission decays fast with a 2.2 day halving timescale, whereas the VHE emission measured by MAGIC is consistent with being constant over the first 4 days and decreasing below the detection limit two weeks later. The $\gamma$-ray emission detected by H.E.S.S. shows a peak with 2 days delay with respect to the GeV emission measured by *Fermi*-LAT. After the moon break without VHE observations, H.E.S.S. still detected a weak ($3\sigma$) signal accumulating 14 days of data.

Both electron and proton acceleration and subsequent emission are possible explanations for the detected HE and VHE signal. When the expanding ejecta of a nova interacts with the interstellar medium — or with the dense wind from a Red Giant in the case of symbiotic novae — a shock wave forms. Additionally, the rapid wind generated by nuclear burning on the white dwarf's surface will eventually collide with the ejecta, creating an internal shock. The recent observations have shown a correlation between optical and gamma-ray emissions, indicating that a significant portion of the nova explosion's energy is channeled into these shocks. These shocks can accelerate electrons and protons to high energies, contributing to the observed emissions. Gamma-ray emission can either originate from thermal radiation at the photosphere, which is upscattered to $\gamma$-ray energies by relativistic electrons through inverse Compton scattering. Alternatively, the surrounding material - comprising the nova ejecta and the Red Giant wind - can serve as a target for hadronic interactions of protons or bremsstrahlung radiation from electrons. The maximum energies of these high-energy particles are determined by the efficiency of the acceleration mechanisms, the duration of the nova, and the energy losses due to cooling [67].

In the end, the observations favour a hadronic scenario. First, it is supported by the goodness of fit to the $\gamma$-ray spectra shown in Figure 10. Fitting the spectrum between 50 MeV and 250 GeV is difficult with leptonic processes, they require an ad-hoc strong spectral break. Whereas protons can be injected with standard parameters. Moreover, the spectral hardening and the decrease of the flux normalization with time, visible in Figure 10, right, is in line with the expectations from the cooling and acceleration time scales for protons [66]. Protons undergo relatively mild cooling through proton-proton interactions, while electrons in nova shocks face significant energy losses due to inverse Compton scattering. Consequently, generating high-energy photons through leptonic mechanisms requires a much higher efficiency in the acceleration process compared to proton-based models [67].

The role of Galactic novae regarding CR production is also discussed in [66] and [67]. Protons within the nova shock experience gradual cooling, allowing them to eventually escape the shock and carry away a significant amount of energy. Such protons could contribute to the Galactic Cosmic Ray sea. Using the CR energetics derived for RS Ophiuchi ($\sim 4.4 \times 10^{43}$) results in an overall contribution of <0.2%. Despite the small contribution to the overall Cosmic Ray sea, novae would significantly increase the CR density in its close environment. In cases of recurrent novae, protons will accumulate in a $\sim 10$ pc bubble with enhanced CR density.

### 6.3 Prospects & Open questions

**Are all novae GeV $\gamma$-ray sources?** Within reliable distances it indeed seems that all novae emit GeV $\gamma$-rays. The majority of novae within $\sim 4$ kpc including a subset of novae from the Bulge at $\sim 8$ kpc was detected with the *Fermi*-LAT.

**Was RS Ophiuchi special with respect to other novae?** The question remains why RS Ophiuchi could be detected at VHE energies, whereas others could not. Figure 11 shows comparisons of the GeV spectra from *Fermi*-LAT detected novae and the one from RS Ophiuchi. Furthermore, it compares the total energy as function of the emission duration for several novae. RS Ophiuchi has an almost two orders of magnitude larger flux than previously detected eruptions by the *Fermi*-LAT. However, except for its brightness, the comparisons do not reveal any peculiarity in the emission of RS Ophiuchi [67].

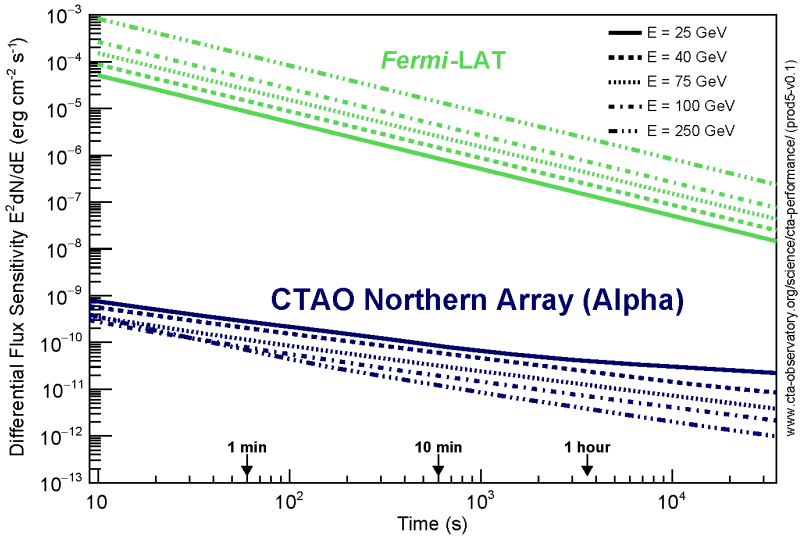


**Figure 12:** Differential flux sensitivity of CTAO-North at selected energies as function of observation time in comparison with the *Fermi*-LAT instrument.

**Are more VHE nova detections to be expected?** T Coronae Borealis (T CrB) is a recurrent symbiotic nova with an expected recurrence period of approximately 80 years and eruptions in 1866 and 1946. Currently, T CrB has entered its distinctive pre-eruption dip and is anticipated to erupt around 2024.4 ± 0.3 years[5]. T CrB is located much closer to Earth (D = 906 pc [72]) compared to RS Ophiuchi (D = 2.69 kpc [72]), making it approximately 2.5 magnitudes brighter in optical. The peak V-band magnitude of RS Ophiuchi was around 5, whereas T CrB is expected to reach a V-band magnitude of about 2.5. This increased brightness will extend to its non-thermal spectrum, enabling a much more detailed study of its non-thermal emission characteristics. Multi-wavelengths instruments world-wide are prepared to swiftly react to the foreseen eruption of this system.

## 7. Summary & Outlook

Galactic transients are a highly dynamic field within high and very high energy astrophysics with continuously upcoming new discoveries. Several newly emerging source classes, such as supernovae and transitional millisecond pulsars at TeV energies, await detection in the coming years. Moreover, 2024 has the potential to significantly boost our understanding of emission processes in novae at TeV energies with the eruption of T Coronae Borealis being one of the most anticipated astronomical event of the year.

More sensitive instruments, such as the Cherenkov Telescope Array Observatory, will soon be operational in the TeV energy range. As illustrated in Figure 12, the full Northern array of CTAO will offer a sensitivity 10,000 times greater than that of *Fermi*-LAT for timescales ranging from minutes to hours. However, it is important to note that CTAO will have a 10% duty cycle

[5]https://www.aavso.org/news/t-crb-pre-eruption-dip

due to weather and light constraints, compared to the 90% duty cycle of Fermi-LAT. Both aspects highlight the complementarity of space and ground-based instruments.

## Acknowledgements

I want to thank the organizers for the perfect conference and for the invitation to give a review talk. Furthermore, I would like to thank the UTokyo Support system for the independence and development of young researchers (The University of Tokyo Excellent Researcher).

## References

[1] Thompson D. J., Wilson-Hodge C. A., 2022, hxga.book, 29.

[2] Aleksić J., Ansoldi S., Antonelli L. A., Antoranz P., Babic A., Bangale P., Barceló M., et al., 2016, APh, 72, 76.

[3] Aharonian F., Akhperjanian A. G., Bazer-Bachi A. R., Beilicke M., Benbow W., Berge D., Bernlöhr K., et al., 2006, A&A, 457, 899.

[4] Holler M., Berge D., van Eldik C., Lenain J.-P., Marandon V., Murach T., de Naurois M., et al., 2015, Proceedings of The 34th International Cosmic Ray Conference — PoS(ICRC2015), 847.

[5] Park N., 2016, Proceedings of The 34th International Cosmic Ray Conference — PoS(ICRC2015), 236, 771.

[6] Lattimer J. M., Prakash M., 2004, Sci, 304, 536.

[7] Bhattacharyya S., Papitto A., Bhattacharya D., 2022, ASSL, 465, 319.

[8] Papitto A., 2022, "Bridging accretion and rotation-powered neutron stars, the case of transitional millisecond pulsars" Presented at the Variable Galactic $\gamma$-Ray Sources (VI), Innsbruck, Austria

[9] Papitto A., Ferrigno C., Bozzo E., Rea N., Pavan L., Burderi L., Burgay M., et al., 2013, Nature, 501, 517.

[10] Torres D. F., Ji L., Li J., Papitto A., Rea N., de Oña Wilhelmi E., Zhang S., 2017, ApJ, 836, 68.

[11] Aliu E., Archambault S., Archer A., Benbow W., Bird R., Biteau J., Buchovecky M., et al., 2016, ApJ, 831, 193.

[12] Turolla R., Esposito P., 2013, IJMPD, 22, 1330024-163.

[13] Esposito P., Rea N., Israel G. L., 2021, ASSL, 461, 97.

[14] Kaspi V. M., Beloborodov A. M., 2017, ARA&A, 55, 261.

[15] Roberts O. J., Veres P., Baring M. G., Briggs M. S., Kouveliotou C., Bissaldi E., Younes G., et al., 2021, Nature, 589, 207.

[16] *Fermi*-LAT Collaboration, Ajello M., Atwood W. B., Axelsson M., Baldini L., Barbiellini G., Baring M. G., et al., 2021, NatAs, 5, 385.

[17] Ashkar H., El Bouhaddouti M., Fegan S. and Schüssler F., PoS ICRC2023 (2023) 555.

[18] Petroff E., Hessels J. W. T., Lorimer D. R., 2019, A&ARv, 27, 4.

[19] Petroff E., Hessels J. W. T., Lorimer D. R., 2022, A&ARv, 30, 2.

[20] Scholz P. on behalf of CHIME/FRB Collaboration, 2020, ATel, 13681

[21] CHIME/FRB Collaboration, Andersen B. C., Bandura K. M., Bhardwaj M., Bij A., Boyce M. M., Boyle P. J., et al., 2020, Nature, 587, 54.

[22] Lin L., Zhang C. F., Wang P., Gao H., Guan X., Han J. L., Jiang J. C., et al., 2020, Nature, 587, 63.

[23] Zhou P., Zhou X., Chen Y., Wang J.-S., Vink J., Wang Y., 2020, ApJ, 905, 99.

[24] Zhang B., 2020, Nature, 587, 45.

[25] Lyubarsky Y., 2014, MNRAS, 442, L9.

[26] Murase K., Kashiyama K., Mészáros P., 2016, MNRAS, 461, 1498.

[27] Metzger B. D., Fang K., Margalit B., 2020, ApJL, 902, L22.

[28] López-Oramas A., Jiménez Martínez I., Hassan T., Hoang J., Inoue S., The MAGIC Collaboration, Acciari V. A., et al., 2022, icrc.conf, 783.

[29] Kostunin D., 2021, Proceedings of The 37th International Cosmic Ray Conference — PoS(ICRC2021), 395, 777.

[30] Kaspi V. M., Beloborodov A. M., 2017, ARA&A, 55, 261.

[31] H.E.S.S. Collaboration, 2019, "Core-collapse supernovae: promising candidates for PeV cosmic-ray acceleration?", https://www.mpi-hd.mpg.de/HESS/pages/home/som/2019/07/.

[32] H. E. S. S. Collaboration, Abdalla H., Aharonian F., Ait Benkhali F., Angüner E. O., Arakawa M., Arcaro C., et al., 2019, A&A, 626, A57.

[33] Murase K., Thompson T. A., Lacki B. C., Beacom J. F., 2011, PhRvD, 84, 043003.

[34] Bell A. R., Schure K. M., Reville B., Giacinti G., 2013, MNRAS, 431, 415.

[35] Cristofari P., Marcowith A., Renaud M., Dwarkadas V. V., Tatischeff V., Giacinti G., Peretti E., et al., 2022, MNRAS, 511, 3321.

[36] Brose R., Sushch I., Mackey J., 2022, MNRAS, 516, 492.

[37] Ptuskin V. S., Zirakashvili V. N., 2005, A&A, 429, 755.

[38] Cardillo M., Amato E., Blasi P., 2015, APh, 69, 1.

[39] Marcowith A., Dwarkadas V. V., Renaud M., Tatischeff V., Giacinti G., 2018, MNRAS, 479, 4470.

[40] Arnett W. D., Bahcall J. N., Kirshner R. P., Woosley S. E., 1989, Annu. Rev. Astron. Astrophys., 27, 629.

[41] Frank K. A., Zhekov, S. A., Park S., McCray R., Dwek E. and Burrows D. N., 2016, ApJ, 829, 1.

[42] Berezhko, E. G.; Ksenofontov, L. T.; Völk, H. J., 2015, ApJ, 810, 63B.

[43] H.E.S.S. Collaboration et al., 2015, Science, 347, 406.

[44] Ackermann M. et al., 2016, A&A, 586, A71.

[45] Malyshev D., Pühlhofer G., Santangelo A., Vink J., 2019, arXiv, arXiv:1903.03045.

[46] H. E. S. S. Collaboration, Abdalla H., Aharonian F., Ait Benkhali F., Angüner E. O., Arakawa M., Arcaro C., et al., 2019, A&A, 626, A57.

[47] Dwarkadas, V. V. 2013, MNRAS, 434, 3368.

[48] Ackermann M. et al. 2015, ApJ, 807, 169.

[49] Yuan Q., Liao N.-H., Xin Y.-L., Li Y., Fan Y.-Z., Zhang B., Hu H.-B., et al., 2018, ApJL, 854, L18.

[50] Xi S.-Q., Liu R.-Y., Wang X.-Y., Yang R.-Z., Yuan Q., Zhang B., 2020, ApJL, 896, L33.

[51] Bianciardi G., Ciccarelli A. M., Conzo G., D'Angelo M., Ghia S., Moriconi M., Orbanić Z., et al., 2023, TNSAN, 213.

[52] Yamanaka M., Fujii M., Nagayama T., 2023, PASJ, 75, L27.

[53] Chandra P., Maeda K., Chevalier R. A., Nayana A. J., Ray A., 2023, ATel, 16073

[54] Marti-Devesa G., 2023, ATel, 16075

[55] Ahnen M. L., Ansoldi S., Antonelli L. A., Antoranz P., Arcaro C., Babic A., Banerjee B., et al., 2017, A&A, 602, A98.

[56] Gal-Yam A., 2019, ARA&A, 57, 305.

[57] Acharyya A., Adams C. B., Bangale P., Benbow W., Buckley J. H., Capasso M., Dwarkadas V. V., et al., 2023, ApJ, 945, 30.

[58] Cristofari P., Marcowith A., Renaud M., Dwarkadas V. V., Tatischeff V., Giacinti G., Peretti E., et al., 2022, MNRAS, 511, 3321.

[59] Brose R., Sushch I., Mackey J., 2022, MNRAS, 516, 492.

[60] Chomiuk L., Metzger B. D., Shen K. J., 2021, ARA&A, 59, 391.

[61] Tatischeff V., Hernanz M., 2007, ApJL, 663, L101.

[62] Abdo A. A., Ackermann M., Ajello M., Atwood W. B., Baldini L., Ballet J., Barbiellini G., et al., 2010, Sci, 329, 817.

[63] Aliu E., Archambault S., Arlen T., Aune T., Beilicke M., Benbow W., Bouvier A., et al., 2012, ApJ, 754, 77.

[64] Franckowiak A., Jean P., Wood M., Cheung C. C., Buson S., 2018, A&A, 609, A120.

[65] Ahnen M. L., Ansoldi S., Antonelli L. A., Antoranz P., Babic A., Banerjee B., Bangale P., et al., 2015, A&A, 582, A67.

[66] H. E. S. S. Collaboration, Aharonian F., Ait Benkhali F., Angüner E. O., Ashkar H., Backes M., Baghmanyan V., et al., 2022, Sci, 376, 77.

[67] Acciari V. A., Ansoldi S., Antonelli L. A., Arbet Engels A., Artero M., Asano K., Baack D., et al., 2022, NatAs, 6, 689.

[68] Kobayashi Y. et al., PoS ICRC2023 (2023) 677.

[69] Schaefer B. E., 2022, MNRAS, 517, 6150.

[70] Geary, K. Outburst of RS Ophiuchi. VSNET-alert 2021, 26131.

[71] Cheung C. C., Ciprini S., Johnson T. J., 2021, ATel, 14834

[72] van Leeuwen F., de Bruijne J., Babusiaux C., Busso G., Castañeda J., Ducourant C., Fabricius C., et al., 2022, gdr3.rept